Published in final edited form as:
J Control Release. 2014 January 10; 173: . doi:10.1016/j.jconrel.2013.10.031.

Treatment of cancer micrometastasis using a multicomponent chain-like nanoparticle

Pubudu M. Peiris[1,2,3,†], **Randall Toy**[1,3,†], **Aaron Abramowski**[3,4], **Pete Vicente**[1,3], **Samantha Tucci**[1,3], **Lisa Bauer**[3,5], **Aaron Mayer**[1,3], **Morgan Tam**[1,3], **Elizabeth Doolittle**[1,3], **Jenna Pansky**[3,4], **Emily Tran**[1,3], **Dishen Lin**[1,3], **William P. Schiemann**[6], **Ketan B. Ghaghada**[7,8], **Mark A. Griswold**[2,3], and **Efstathios Karathanasis**[1,2,3,6,*]

[1]Department of Biomedical Engineering, Case Western Reserve University, Cleveland, Ohio 44106

[2]Department of Radiology, Case Western Reserve University, Cleveland, Ohio 44106

[3]Case Center for Imaging Research, Case Western Reserve University, Cleveland, Ohio 44106

[4]Department of Biochemistry, Case Western Reserve University, Cleveland, Ohio 44106

[5]Department of Physics, Case Western Reserve University, Cleveland, Ohio 44106

[6]Case Comprehensive Cancer Center, Case Western Reserve University, Cleveland, Ohio 44106

[7]Edward B. Singleton Department of Pediatric Radiology, Texas Children's Hospital, Houston, Texas 77030

[8]Department of Radiology, Baylor College of Medicine, Houston, Texas 77030

Abstract

While potent cytotoxic agents are available to oncologists, the clinical utility of these agents is limited due to their non-specific distribution in the body and toxicity to normal tissues leading to use of suboptimal doses for eradication of metastatic disease. Furthermore, treatment of micrometastases is impeded by several biobarriers, including their small size and high dispersion to organs, making them nearly inaccessible to drugs. To circumvent these limitations in treating metastatic disease, we developed a multicomponent, flexible chain-like nanoparticle (termed nanochain) that possesses a unique ability to gain access to and be deposited at micrometastatic sites. Moreover, coupling nanochain particles to radiofrequency (RF)-triggered cargo delivery facilitated widespread delivery of drug into hard-to-reach cancer cells. Collectively, these features synergistically facilitate effective treatment and ultimately eradication of micrometastatic disease using a low dose of a cytotoxic drug.

Keywords

Chain-like nanoparticle; targeting; cancer metastasis; nanochains; radiofrequency-triggered drug release

[*]Author to whom correspondence should be addressed: Efstathios Karathanasis, 2071 Martin Luther King Jr. Drive, Wickenden Building, Cleveland, Ohio 44106, USA, Phone: +1-216.844.5281; Fax: +1-216.844.4987; stathis@case.edu.
[†]These authors contributed equally to this work

1. INTRODUCTION

The vast majority of breast cancer mortality is due to metastatic disease [1]. For example, the 5-year survival rate of breast cancer patients sharply decreases from 98% in cases with localized primary lesions to 23% in cases of distant metastases [1]. Although oncologists have potent small molecule chemotherapeutics such as anthracyclines (*e.g.* doxorubicin; abbreviated as DOX), the dose of these agents is constrained by their toxicity to normal tissue, because they are distributed within cancer and healthy tissues in a non-specific manner [2].

Due to the unique structures and material properties that appear at the nano-scale, nanoparticles provide new opportunities to address the complexity of cancer metastasis. To date, though, applications of nanotechnology have mainly focused on primary tumors. Nanoparticles have been developed to exploit the leaky vasculature of primary tumors to enhance the intratumoral drug delivery due to the so-called 'Enhanced Permeability and Retention' (EPR) effect [3–7]. While the EPR strategy may be effective in well-vascularized tumors larger than 100 mm^3, it is ineffective in micrometastatic disease, which presents small clusters of malignant cells within variable tissue types [8, 9]. However, targeting an occult lesion hidden within a large population of normal cells presents a unique challenge [8].

To overcome these limitations of current drugs in their molecular or nanoparticle form, we designed a multicomponent nanochain (termed nChain), which is comprised of three iron oxide (IO) nanospheres and one drug-loaded liposome chemically linked into a linear, chain-like assembly (Fig. 1a,b). The multicomponent nature and shape of the nChain particle result in two unique features that facilitate enhanced treatment of difficult-to-reach cancer sites. The micrometastasis-specific features of the nChain-based therapy are illustrated in Fig. 1c. First, the nChain particle is capable of transporting a large drug cargo to metastases *via* vascular targeting of the endothelium associated with micrometastasis. The nChain utilizes a cyclic RGD peptide as a ligand to target the $\alpha_v\beta_3$ integrin receptor, which has a well-established role in the development of breast cancer metastasis [10–16]. While initial adhesion of circulating tumor cells onto the endothelium involves cell rolling, the metastatic site quickly transitions to firm attachment that is mediated by $\alpha_v\beta_3$ integrin [10, 12–15]. Although $\alpha_v\beta_3$ integrin mediates the adhesion of cells to a large number of extracellular matrix proteins, it is minimally expressed on normal blood vessels [17–19]. Thus, $\alpha_v\beta_3$ integrin-mediated vascular targeting can be highly specific towards blood vessels associated with metastatic disease, particularly since extravascular metastases are preceded by metastatic cancer cells residing inside the lumen of blood vessels [10, 20, 21]. Furthermore, the size, shape and flexibility of nChain particles substantially increase their probability of homing to micrometastases. The structure of the nChain particle increases both the lateral drift and margination of nanoparticles towards the blood vessel walls in microcirculation (*i.e.* continuous scavenging of vascular walls), and targeting avidity of nanoparticles (*i.e.* latching on vascular target) due to geometrically enhanced multivalent attachment on the vascular target [22].

However, even after successful targeting of a nanoparticle to micrometastasis, the overall effectiveness of this event primarily reflects the biological activity of "free" drug against neighboring cancer cells. While nanoparticles typically release their content slowly, drug release from nChain particles can be remotely triggered due to mechanically induced defects of the liposomal membrane caused by the oscillation of the IO portion of the nChain in the presence of a mild radiofrequency (RF) field [19]. For these analyses, we chose the drug DOX, which can rapidly diffuse through cellular membranes and reach nuclear DNA, which

functions as a sink for DOX [23–25]. Application of an RF field rapidly liberated DOX molecules from nChain particles resulting in widespread anticancer activity throughout micrometastatic sites.

2. MATERIALS AND METHODS

2.1. Materials

The 4T1-GFP-luc cell line was received as a gift from Dr. Ruth Keri (Case Western Reserve University, Cleveland, OH). Female Balb/c mice were purchased from Charles Rivers (Wilmington, MA). The primary antibody for the specific endothelial antigen CD31 was purchased from BD Biosciences Pharmingen (San Diego, CA). Secondary antibodies and cell culture media were obtained from Invitrogen (Carlsbed, CA). The TUNEL assay kit was obtained from purchased from Roche Diagnostics (Indianapolis, IN). Cross-Linked Ethoxylate Acrylate Resin (CLEAR) resin, reaction vessels, other accessories for solid-phase chemistry and the cyclo (Arg-Gly-Asp-D-Phe-Cys) or c(RGDfC) peptide were purchased from Peptides International Inc (Louisville, KY). The crosslinkers 3,3′-Dithiobis(sulfosuccinimidylpropionate) (DTSSP) and sulfosuccinimidyl 4-[N-maleimidomethyl]cyclohexane-1-carboxylate (sulfo-SMCC), and the cleaving agent Tris[2-carboxyethyl] phosphine (TCEP) were obtained from Thermo Fisher Scientific (Cleveland, OH). Polyethylene glycol (PEG) conjugates were purchased from Laysan Bio (Arab, AL). General solvents and chemicals were obtained from Thermo Fisher Scientific (Cleveland, OH). Doxorubicin (DOX) was obtained from Sigma (Saint Louis, MO).

2.2. Synthesis and characterization of nanoparticles

To fabricate the multicomponent nChain particles, we employed a stepwise solid-phase chemistry approach to assemble the particles following a modification of a previously published method [19, 26]. In the first step, solid-phase chemistry was used to partially modify the surface functionality of IO nanospheres with a hydrodynamic diameter of 27 nm (the size of the IO core is 10 nm) (Fig. 2a). Amine-PEG-functionalized IO nanospheres were conjugated onto amine-functionalized CLEAR resin *via* a homobifunctional crosslinker (DTSSP) reactive towards amines containing a cleavable disulfide bridge. The IO nanospheres were allowed to bind to the solid support and then cleaved off using a reducing agent (TCEP). The thiolytic cleavage liberated the IO nanosphere from the solid support converting the amines to a different chemical functionality (thiol group) on the portion of the nanosphere's surface that was linked to the resin. In the second step, by defining the topology of two different functional groups on the surface of the parent nanospheres, the two unique faces on the parent IO nanosphere served as fittings to chemically assemble them into nanochains using solid-phase chemistry (Fig. 2b). The same type of resin was used and the modified nanospheres were introduced in a step-by-step manner using a heterobifunctional crosslinker with NHS-MAL functionality (sulfo-SMCC). It should be noted that each step included multiple washing/drying cycles to remove any unbound nanospheres and excess reagents from the nanoparticle-resin complex. As a final component, an amine functionalized DOX-loaded liposome with a hydrodynamic diameter of 35 nm was added. The liposomes were prepared by sequential extrusion through a 50 nm filter followed by sonication for 30 min at 30ºC. DOX was remotely loaded to the liposomes against an ammonium sulfate gradient [27]. The thiol of the cysteine residue of the c(RGDfC) peptide was used to conjugate the targeting ligand to the remaining amine-terminated PEG on the surface of nChain particles. Finally, the $\alpha_v\beta_3$ integrin-targeting nChain particles were cleaved off the resin and recovered.

The nanoparticles were characterized in terms of their size using a ZetaPALS dynamic light scattering system (DLS; Brookhaven Instruments, Holtsville, NY). TEM images were

obtained using a Tecnai F30 instrument (FEI, Hillsboro, OR) operated at 300 kV. The concentration of iron was determined *via* ICP-OES (Optima 7000 DV; Perkin-Elmer, Waltham, MA). Due to the simplified purification procedure and easy handling of multiple reaction vessels, the solid-phase-based synthesis enabled us to manufacture large amounts of nChain particles that exhibited a high degree of uniformity with the majority of the particles (73%) comprised of three IO nanospheres and one liposome [19, 22]. Due to the high intraliposomal space available for drug encapsulation and the efficient remote loading technique (entrapment efficiency was ~95% of the initial amount of DOX added to the liposomal suspension) [27], the drug cargo was high (6.8×10^{-5} ng DOX per nChain particle). More detailed characterization of the nanochain particles can be found in previous publications [19, 26].

In order to assess the *in vivo* performance of the nChain particles, we compared them to other control formulations using different therapeutic protocols, which are summarized in Table 1.

2.3. Tumor model

All animal procedures were conducted under a protocol approved by the CWRU IACUC. We used the orthotopic 4T1-luc-GFP breast tumor model in mice [19, 22]. Using flow cytometry and antibodies specific to the α_v and β_3 subunits, previous studies have shown the overexpression of $\alpha_v\beta_3$ integrin in the 4T1 cell line [28]. The 4T1-luc-GFP cell line was engineered to stable express firefly luciferase and green fluorescent protein (GFP). Briefly, we inoculated 0.5×106 4T1-luc-GFP cells orthotopically in a no. 9 mammary fat pad of female BALB/c mice that was surgically exposed while mice were anesthetized. We have previously established that disseminated metastases are developed within 14 days of 4T1 inoculation. At that point, the primary tumor was resected using established methods [29]. The animals were used 5 days after surgery to allow the animals to recover.

2.4. Biophotonic *in vivo* imaging

Starting at 10 days after tumor inoculation, 200 μl of D-luciferin (10 mg/ml) were intraperitoneally administered and imaged after 10 min using Bioluminescence Imaging (BLI) with a preclinical In Vivo Imaging System (IVIS, Perkin Elmer, Waltham, MA). The animals were imaged every 3–5 days until the terminal point of the study. At the endpoint, organs were extracted and processed for histological analysis. The time-course of cancer progression was obtained by quantification of the whole body BLI signal, which was normalized to the background signal of healthy animals.

2.5. Survival study

The animals were injected with nChain *via* tail vein at a dose of 0.5 mg/kg DOX 19 days after tumor inoculation. A 60-min application of the RF field (amplitude B=2 mT, frequency f=10 kHz, RF power=3–5 Watts) was employed 45 min after injection, using a custom-made solenoid (N=105 turns, Inner Diameter=2.8 cm) [19]. The RF coil was positioned 1 cm from the animal and oriented such that the magnetic field was directed toward the abdominal and thoracic region. During this procedure the animals were anesthetized through the administration of inhalant isoflurane. Three subsequent treatments were applied at time intervals of three days. Following the same dose and schedule, control groups included untreated animals and animals treated with DOX followed by RF, targeting liposomes followed by RF, and nChain. In addition to BLI imaging, the tumor growth was allowed to progress until the animals showed changes in grooming, weight, behaviors, at which point animals were euthanized in a CO_2 chamber. Time of death was determined to be the following day.

2.6. Fluorescence *in vivo* imaging

This study was performed at 25 days after tumor inoculation. Following identification of lung metastasis using BLI imaging, Fluorescence Molecular Tomography (FMT) imaging was performed at multiple time points after injection (t=0, 30 min and 2, 5, 24 hours) of nChain, targeting liposomes and non-targeting liposomes at a dose of 0.5 mg/kg DOX. Each nanoparticle formulation was labeled with an NIR fluorescent dye (Vivotag 680). Phantoms for each formulation were used to calibrate the FMT to take quantitative deposition measurements of regions of interest containing lung metastasis. Organs from animals injected with saline were also imaged to determine background fluorescence at all excitation wavelengths. To verify the findings of the *in vivo* imaging, organs were imaged *ex vivo* using a CRi Maestro fluorescence imaging system.

2.7. Histological evaluation

Animals were injected with nChain and targeting liposomes at 25 days after tumor inoculation. Animals were euthanized at either 30 min, 120 min or 48 h post-injection. Briefly, the animals were anesthetized with an IP injection of ketamine/xylazine and transcardially perfused with heparinized PBS followed by 4% paraformaldehyde in PBS. Organs were explanted and processed for cryosectioning. Serial tissue sections of 12-μm thickness were stained for the specific endothelial antigen CD31 and with the nuclear stain DAPI. The tissue sections were imaged at 5, 10 and 20x magnification on the Zeiss Axio Observer Z1 motorized FL inverted microscope. To obtain an image of an entire large section of an organ (*e.g.* liver lobe), a montage of each section was made using the automated tiling function of the microscope. Direct fluorescence (red) imaging was used for DOX. Direct fluorescence of GFP (green) imaging was performed for imaging the location of metastatic lesions. Apoptotic cells were identified based on TUNEL-stained nuclei.

2.8. Statistical analysis

Means were determined for each variable in this study and the resulting values from each experiment were subjected to one-way analysis of variance with post hoc Bonferroni test (SPSS 15, Chicago, IL). A P value of less than 0.05 was used to confirm significant differences. Normality of each data set was confirmed using the Anderson-Darling test.

3. RESULTS

3.1. *In vivo* evaluation of nChain's ability to target metastasis

To evaluate the nChain's efficiency at seeking micrometastasis, we compared the nChain particles to $\alpha_v\beta_3$ integrin-targeting 30-nm liposomes (termed Lip) and their non-targeting variant (termed NT-Lip) in their ability to target micrometastasis in lungs. In these studies, we used the murine 4T1 breast cancer cells, which represent a model of triple-negative breast cancer (TNBC). The 4T1 cells are syngeneic with Balb/C mice, thereby facilitating studies of TNBC development in immunocompetent mice, which ultimately develop metastases at organ sites reminiscent of those observed in human patients [29–34]. In order to more carefully recapitulate clinical breast cancer settings, we surgically resected primary 4T1 tumors, developed in the mammary fat pad of mice, whose micrometastatic foci remained intact. The stable expression of firefly luciferase of the 4T1-luc-GFP cells enabled longitudinal bioluminescence imaging (BLI) of the location and progression of metastases, which showed that the primary tumor of untreated animals grew rapidly within 12 days after 4T1 cell engraftment (Fig. 3a). While surgical resection of the primary tumor at day 14 resulted in elimination of BLI signal, metastasis quickly became detectable in the thoracic region and primary site followed by rapid spread to the rest of the body.

Following BLI imaging to identify the location of lung metastasis, Fluorescence Molecular Tomography (FMT) was used to noninvasively and quantitatively monitor the accumulation of nanoparticles labeled with an NIR fluorophore in lung metastasis (Fig. 3b and Supplementary Fig. 1a). The nChain particles displayed maximum fluorescence signal in metastases within 2 h post-injection (Fig. 3c). At that time point, vascular targeting of nChain resulted in ~6% of the administered dose being localized in lung metastasis, which was 7.5-fold higher than targeting liposomes. As expected, NT-Lip exhibited negligible accumulation at metastatic sites in the lungs. The *in vivo* FMT imaging-based measurements of nChain concentration were validated by direct measurement of iron concentration in lung tissues of animals using inductively coupled plasma optical emission spectroscopy (ICP-OES). Furthermore, to confirm the localization of nChain in metastasis, lungs were imaged *ex vivo* indicating the colocalization of nChain particles and cancer cells (Fig. 3d). Similar to lungs, *ex vivo* imaging of liver also indicated that nChain particles exhibited highly specific deposition at liver metastasis (Supplementary Fig. 1b) in addition to the typical clearance of nChain particles by macrophages (Supplementary Fig. 2).

3.2. *In vivo* evaluation of nChain's therapeutic efficacy

All the animals selected for this study exhibited comparable progression of metastatic disease in terms of location, size and BLI signal intensity. At 5 days post-surgery, the animals were intravenously injected with nChain. A 60-min application of the RF was employed 45 min after injection (nChain/RF group), which corresponds to the time window of maximum nChain deposition in metastases. Control treatments included free DOX followed by RF (DOX/RF), $\alpha_v\beta_3$ integrin-targeting 30-nm liposomal DOX followed by RF (Lip/RF), and nChain without RF (nChain). The treatments were administered four times (Fig. 4a), each at a dose of 0.5 mg DOX per kg of body weight, which is ~10-fold lower than the typical clinical dosage of liposomal DOX [35, 36]. As shown in representative BLI images (Fig. 4b), the DOX/RF treatment had negligible therapeutic benefits, while nChain (without RF) exhibited a moderate effect. Most importantly, the whole body BLI signal of animals treated with nChain/RF completely disappeared within a few days after initiation of treatment.

As a metric of the response of metastasis to the various treatments (n=7 in each group), quantification of BLI signal was used (Fig. 4c). While the nChain therapy (without RF) decelerated metastatic growth for a few days compared to the DOX/RF and Lip/RF treatments, the growth of metastasis quickly became similar to the untreated group. Importantly, animals treated with nChain/RF exhibited a dramatic decrease of BLI signals that quickly approached baseline levels. The entire nChain/RF group (n=7) displayed no BLI signal until day 54, at which point metastatic disease recurred in a subset of animals (3/7). While 100% of the mice in other groups died within 50 days, 57% of the nChain/RF-treated group was still alive at 150 days (Fig. 4d). The other 43% of the nChain/RF-treated group exhibited an increase in mean survival (68 days) compared to the groups treated with nChain without RF (44.1 days), Lip/RF-treated (35.2 days), DOX/RF (28.5 days) and the untreated group (30.1 days).

3.3. Histological evaluation

To assess the localization of nChain in micrometastasis and the degree and topology of DOX delivery, histological analysis was performed on separate groups of mice 30 min, 120 min and 48 h after injection (n=3 in each group). A representative image of a liver lobe is shown in Fig. 5a displaying the presence of clusters of metastatic cells dispersed in the liver. Notably, 30 min post-injection, nChain accumulated almost exclusively at metastatic sites. Imaging at higher magnification showed that metastatic cancer cells were localized primarily on the endothelial walls (Fig. 5b). Importantly, nChain particles were

predominantly distributed around those same blood vessels colonized by 4T1 cells (Fig. 5c). Application of the RF field 120 min after injection resulted in widespread delivery of DOX at distant cells away from nChain deposits (Fig. 5d). Imaging at higher magnification shows that RF-triggered release resulted in delivery of DOX to cell nuclei (Fig. 5e), while no spread of DOX was observed in the case of nChain-treated animals that were not exposed to RF, since the fluorescence signal of intraliposomal DOX is quenched (Fig. 5f). Most importantly, 48 h after the nChain/RF treatment, DOX was found in the vast majority of cancer cells (Fig. 5g), while most of the cancer cells were apoptotic as gauged by TUNEL staining (inset of Fig. 5g). Contrary to the nChain/RF group, the nChain and Lip/RF treatments exhibited very low DOX delivery to cancer cells and negligible anticancer effect (Fig. 5h,i). Application of the RF field alone had no effect on cancer cells. Similar to liver, histological analysis of lungs showed that the nChain/RF treatment resulted in localization of nanoparticles and widespread delivery of DOX in micrometastatic sites (Supplementary Fig. 3). The *in vivo* anticancer effects of the nChain/RF treatment observed in histology are consistent to cell cytotoxicity studies (Supplementary Fig. 4). While 30-nm liposomal DOX, 100-nm liposomal DOX and nChain without RF exhibited low cytotoxicity (less than 10% relative cytotoxicity), RF-triggered release of DOX from nChain had significant cytotoxic effects (18%), which was similar to the effect of free DOX.

4. DISCUSSION

Breast cancer was selected for this study due to the potential for rapid clinical translation, since it is the most prevalent cancer among women in the US [1]. While systemic chemotherapy, in its adjuvant mode, prevails as the standard treatment for breast cancer, these potent agents are toxic to both normal and cancer tissues leading to use of suboptimal doses for eradication of metastatic disease [2]. Here, we focused on evaluating the therapeutic efficacy of the nChain treatment in the adjuvant mode in an animal model of TNBC. Among the subtypes of breast cancer [37], TNBC is an extremely aggressive, metastatic and difficult-to-treat subtype. Interestingly, although TNBC comprise 15–25% of all invasive breast cancers, this unique breast cancer subtype displays an unusually aggressive metastatic phenotype that results in their disproportional mortality among breast cancer patients [38–40]. This is due to the fact that drugs cannot easily reach micrometastases, which represent small clusters of cancer cells hidden within a large population of normal cells. However, metastases upregulate specific cell-surface molecules that differ from the rest of its host organ. Specifically, following intravasation, $\alpha_v\beta_3$ integrin expression on the circulating tumor cells plays central role in the formation of metastases at a distal site, which makes this integrin a suitable candidate for targeting micrometastasis [10–16, 41–43]. Indeed, in this work, the *in vivo* studies indicate that vascular targeting of $\alpha_v\beta_3$ integrin associated with micrometastasis provides enhanced selectivity. While various receptors have been exploited to target nanoparticles (*e.g.* folate, EGF, HER2, integrin receptors), the preclinical development of these systems has focused on targeting tumors at the primary site. Attention of the field has recently shifted towards metastasis, but there are still few examples of therapeutics for metastases [8, 44].

In order to further enhance the selectivity of vascular targeting, we exploited the engineerability of nanotechnology to control the geometrical shape of nanoparticles. In fact, in the last decade, the field of nanomedicine has recognized that the particle shape governs the navigation of circulating nanoparticles through different biological processes, including intravascular and transvascular transport, and ultimately targeting of difficult-to-reach cancer sites. One of the pivotal steps dictating the transport of flowing nanoparticles is their margination (*i.e.* radial drift) towards the blood vessel walls. In the case of vascular targeting, near-the-wall margination is not just desirable, but it is required for a nanoparticle to interact with the tumor vascular bed and have subsequent meaningful interactions.

Nanoparticle margination is dictated by forces, which influence particle translational and rotational motion, including buoyancy, gravity, drag, van der Waals interactions, electrostatic double layer interactions, and steric repulsive interactions. Under a balance of these forces, spherical nanoparticles tend to follow blood flow [45, 46]. Contrary to spherical nanoparticles, oblong-shaped nanoparticles are subjected to torques resulting in tumbling and rotation, which increase the lateral drift of nanoparticles towards the blood vessel walls in microcirculation [47–49]. Furthermore, the particle shape also governs the specificity of targeting nanoparticles using receptor-ligand systems. Compared to nanospheres, oblong-shaped nanoparticles exhibit substantially enhanced targeting avidity due to geometrically enhanced multivalent docking, which can effectively offset hemodynamic forces that tend to detach the nanoparticle from the endothelium [22, 50]. Not surprisingly, our *in vivo* studies showed that an outstanding 6% of the administered nChain particles accumulated in micrometastases within 2 h after injection. Furthermore, similar to any type of nanoparticles carrying a cytotoxic agent, the biodistribution of the nChain particles to the major organs is important to assess. The accumulation of nChain in the heart, lungs, brain and kidney 24 h after administration was about 3.5, 3, 2 and 6% of the injected dose, respectively (Supplementary Fig. 2). As expected, the majority of nChain particles was found in the reticuloendothelial organs (liver and spleen). In a previous study [19], we showed that the overall biodistribution of nanochains was comparable to the behavior of the 100-nm liposomal DOX.

Even with that enhanced deposition in metastases, the nChain treatment (without RF) provided only modest benefits. This is primarily related to the drug release profile from nanoparticles. While free drug in its molecular form quickly spreads within the tumor interstitium [23–25], nanoparticles release their content at a relatively slow rate, once they deposit at the target site. This slow release generates a low temporal and spatial concentration gradient of the drug, resulting in non-cytotoxic levels of the drug distal from the particle [25]. Although the slow release of drug from nanoparticles does not favor cytotoxic effects, it improves the drug's safety profile during the particle's circulation in the blood. Thus, our objective was to couple the high selectivity of vascular targeting to a unique triggered drug release mechanism to deliver and spread the drug cargo at cytotoxic levels throughout the hard-to-reach micrometastatic sites. Contrary to heat-induced drug release achieved by other nanoparticle designs (*e.g.* thermosensitive nanoparticles) [51], the release mechanism of nChain particles is concentration-independent resulting in efficient drug release even from very low concentration of nanoparticles [19]. In a previous publication [19], we showed that through their interaction with magnetic fields, the IO component of the nChain particle efficiently converts magnetic energy to mechanical energy resulting in "mechanical" disruption of the liposomal membrane. When magnetic nanoparticles are subjected to an external, oscillating magnetic field, there are two relaxation mechanisms (Brownian and Néel relaxation) that govern their magnetization response in an effort to align with the applied field. Brownian relaxation is typically the dominant relaxation mechanism for nanoparticles larger than about 25 nm. In the case of nChain, Brownian relaxation is restricted by the bonds between the constituent nanospheres, such that Brownian motion may be observed as a mechanical "vibration" of the chain, rather than true rotational motion. Regarding Néel relaxation, to reorient its magnetic moment with an applied field, the nanoparticle must overcome an energy barrier, which results in dissipation of excess heat, which has been exploited for hyperthermia applications. However, our studies showed that no local heating is generated around the nChain particle as a response to the 10 kHz field and that mechanical vibration at the selected frequency is the primary mechanism of drug release.

Indeed, the application of RF on nChain-treated animals significantly impacted the progression of metastasis and, in most cases, resulted in eradication of metastatic disease.

Due to the highly selective deposition of the nChain particles at metastases and subsequently efficient spreading of drug, this significant therapeutic outcome was achieved at a very low dose (*i.e.* 0.5 mg/kg), which is 10–20-fold lower than the typical clinical regimens of liposomal DOX [35, 36]. Thus, both the particle shape and the multicomponent nature of the nChain played an essential role in its therapeutic efficacy.

Historically, attempts to improve nanoparticle homing to tumors have relied on the EPR effect and targeting of various receptors to direct drugs to the primary site. In this study, we show that an integrin-targeting nChain coupled with a vascular targeting strategy and RF-triggered drug release provides an increased likelihood of highly effective treatment of micrometastasis using a low dose of chemotherapy. We envision that successful clinical translation of the nChain particle will provide a powerful chemotherapeutic agent that can be used in the standard adjuvant setting for the majority of breast cancer patients. Considering that expression of $\alpha_v\beta_3$ integrin plays central role in the development and progression of metastasis in melanomas, prostate, pancreatic and cervical cancers [16], vascular targeting of $\alpha_v\beta_3$ integrin appears to be possible for other types of cancer. Taking into consideration that RF can penetrate deep into tissues, the nChain therapeutic could be employed not only for breast cancer but for diverse types of cancer that display aggressive and metastatic phenotypes including cancers of the gastrointestinal tract, lung, prostate, brain.

Supplementary Material

Refer to Web version on PubMed Central for supplementary material.

Acknowledgments

This work was supported by grants from the National Cancer Institute (R01CA177716), the Clinical and Translational Science Collaborative of Cleveland (UL1TR000439) from the National Center for Advancing Translational Sciences component of the National Institutes of Health, the Case Comprehensive Cancer Center (P30CA043703), and the Ohio Cancer Research Associates (E.K.). R.T. was supported by a fellowship from the NIH Interdisciplinary Biomedical Imaging Training Program (T32EB007509), and L.B. was supported by a fellowship from the National Cancer Institute Training Program in Cancer Pharmacology (R25CA148052). We would like to acknowledge Dr. Ruth Keri for providing the 4T1-luc-GFP cell line. We would also like to acknowledge Erik Schmidt for help with the fabrication of nanochains and Avik Banerjee, Dishen Lin, Kaitlyn Murray, Swetha Rao, Christopher Shoup and Sohaj Singh for help with animal studies and histology.

References

1. American Cancer Society. Detailed Guide: Breast Cancer. 2012
2. Von Hoff DD, Layard MW, Basa P, Davis HL Jr, Von Hoff AL, Rozencweig M, Muggia FM. Risk factors for doxorubicin-induced congestive heart failure. Ann Intern Med. 1979; 91:710–717. [PubMed: 496103]
3. Maeda H, Wu J, Sawa T, Matsumura Y, Hori K. Tumor vascular permeability and the EPR effect in macromolecular therapeutics: a review. J Control Release. 2000; 65:271–284. [PubMed: 10699287]
4. Gradishar WJ, Tjulandin S, Davidson N, Shaw H, Desai N, Bhar P, Hawkins M, O'Shaughnessy J. Phase III trial of nanoparticle albumin-bound paclitaxel compared with polyethylated castor oil-based paclitaxel in women with breast cancer. J Clin Oncol. 2005; 23:7794–7803. [PubMed: 16172456]
5. Lasic DD. Doxorubicin in sterically stabilized liposomes. Nature. 1996; 380:561–562. [PubMed: 8606781]
6. Lasic DD, Papahadjopoulos D. Liposomes revisited. Science. 1995; 267:1275–1276. [PubMed: 7871422]
7. Safra T. Cardiac safety of liposomal anthracyclines. Oncologist. 2003; 8(Suppl 2):17–24. [PubMed: 13679592]

8. Schroeder A, Heller DA, Winslow MM, Dahlman JE, Pratt GW, Langer R, Jacks T, Anderson DG. Treating metastatic cancer with nanotechnology. Nat Rev Cancer. 2012; 12:39–50. [PubMed: 22193407]
9. Adiseshaiah PP, Hall JB, McNeil SE. Nanomaterial standards for efficacy and toxicity assessment. Wiley Interdiscip Rev Nanomed Nanobiotechnol. 2010; 2:99–112. [PubMed: 20049834]
10. Gay LJ, Felding-Habermann B. Contribution of platelets to tumour metastasis. Nat Rev Cancer. 2011; 11:123–134. [PubMed: 21258396]
11. Felding-Habermann B, Habermann R, Saldivar E, Ruggeri ZM. Role of beta3 integrins in melanoma cell adhesion to activated platelets under flow. J Biol Chem. 1996; 271:5892–5900. [PubMed: 8621462]
12. McCarty OJ, Mousa SA, Bray PF, Konstantopoulos K. Immobilized platelets support human colon carcinoma cell tethering, rolling, and firm adhesion under dynamic flow conditions. Blood. 2000; 96:1789–1797. [PubMed: 10961878]
13. Arnaout MA, Mahalingam B, Xiong JP. Integrin structure, allostery, and bidirectional signaling. Annu Rev Cell Dev Biol. 2005; 21:381–410. [PubMed: 16212500]
14. Felding-Habermann B, O'Toole TE, Smith JW, Fransvea E, Ruggeri ZM, Ginsberg MH, Hughes PE, Pampori N, Shattil SJ, Saven A, Mueller BM. Integrin activation controls metastasis in human breast cancer. Proc Natl Acad Sci U S A. 2001; 98:1853–1858. [PubMed: 11172040]
15. Lorger M, Krueger JS, O'Neal M, Staflin K, Felding-Habermann B. Activation of tumor cell integrin alphavbeta3 controls angiogenesis and metastatic growth in the brain. Proc Natl Acad Sci U S A. 2009; 106:10666–10671. [PubMed: 19541645]
16. Desgrosellier JS, Cheresh DA. Integrins in cancer: biological implications and therapeutic opportunities. Nat Rev Cancer. 2010; 10:9–22. [PubMed: 20029421]
17. Brooks PC, Clark RA, Cheresh DA. Requirement of vascular integrin alpha v beta 3 for angiogenesis. Science. 1994; 264:569–571. [PubMed: 7512751]
18. Brooks PC, Stromblad S, Klemke R, Visscher D, Sarkar FH, Cheresh DA. Antiintegrin alpha v beta 3 blocks human breast cancer growth and angiogenesis in human skin. J Clin Invest. 1995; 96:1815–1822. [PubMed: 7560073]
19. Peiris PM, Bauer L, Toy R, Tran E, Pansky J, Doolittle E, Schmidt E, Hayden E, Mayer A, Keri RA, Griswold MA, Karathanasis E. Enhanced Delivery of Chemotherapy to Tumors Using a Multicomponent Nanochain with Radio-Frequency-Tunable Drug Release. ACS Nano. 2012; 6:4157–4168. [PubMed: 22486623]
20. Zhang Q, Yang M, Shen J, Gerhold LM, Hoffman RM, Xing HR. The role of the intravascular microenvironment in spontaneous metastasis development. Int J Cancer. 2010; 126:2534–2541. [PubMed: 19847811]
21. Steeg PS, Camphausen KA, Smith QR. Brain metastases as preventive and therapeutic targets. Nat Rev Cancer. 2011; 11:352–363. [PubMed: 21472002]
22. Peiris PM, Toy R, Doolittle E, Pansky J, Abramowski A, Tam M, Vicente P, Tran E, Hayden E, Camann A, Mayer A, Erokwu BO, Berman Z, Wilson D, Baskaran H, Flask CA, Keri RA, Karathanasis E. Imaging metastasis using an integrin-targeting chain-shaped nanoparticle. ACS Nano. 2012; 6:8783–8795. [PubMed: 23005348]
23. Terasaki T, Iga T, Sugiyama Y, Sawada Y, Hanano M. Nuclear binding as a determinant of tissue distribution of adriamycin, daunomycin, adriamycinol, daunorubicinol and actinomycin D. J Pharmacobiodyn. 1984; 7:269–277. [PubMed: 6470925]
24. Marafino BJ Jr, Giri SN, Siegel DM. Pharmacokinetics, covalent binding and subcellular distribution of [3H]doxorubicin after intravenous administration in the mouse. J Pharmacol Exp Ther. 1981; 216:55–61. [PubMed: 7452508]
25. Laginha KM, Verwoert S, Charrois GJ, Allen TM. Determination of doxorubicin levels in whole tumor and tumor nuclei in murine breast cancer tumors. Clin Cancer Res. 2005; 11:6944–6949. [PubMed: 16203786]
26. Peiris PM, Schmidt E, Calabrese M, Karathanasis E. Assembly of linear nano-chains from iron oxide nanospheres with asymmetric surface chemistry. PLoS One. 2011; 6:e15927. [PubMed: 21253600]

27. Bolotin E, Cohen R, Bar L, Emanuel N, Ninio S, Lasic D, Barenholz Y. Ammonium sulfate gradients for efficient and stable remote loading of amphipathic weak bases into liposomes and ligandoliposomes. Journal of Liposome Research. 1994; 4:455–479.
28. Sloan EK, Pouliot N, Stanley KL, Chia J, Moseley JM, Hards DK, Anderson RL. Tumor-specific expression of alphavbeta3 integrin promotes spontaneous metastasis of breast cancer to bone. Breast Cancer Res. 2006; 8:R20. [PubMed: 16608535]
29. Pulaski BA, Ostrand-Rosenberg S. Mouse 4T1 breast tumor model. Curr Protoc Immunol, Chapter. 2001; 20(Unit 20):22.
30. Tao K, Fang M, Alroy J, Sahagian GG. Imagable 4T1 model for the study of late stage breast cancer. BMC Cancer. 2008; 8:228. [PubMed: 18691423]
31. Dykxhoorn DM, Wu Y, Xie H, Yu F, Lal A, Petrocca F, Martinvalet D, Song E, Lim B, Lieberman J. miR-200 enhances mouse breast cancer cell colonization to form distant metastases. PLoS One. 2009; 4:e7181. [PubMed: 19787069]
32. Gao ZG, Tian L, Hu J, Park IS, Bae YH. Prevention of metastasis in a 4T1 murine breast cancer model by doxorubicin carried by folate conjugated pH sensitive polymeric micelles. J Control Release. 152:84–89. [PubMed: 21295088]
33. Wendt MK, Molter J, Flask CA, Schiemann WP. In vivo dual substrate bioluminescent imaging. J Vis Exp.
34. Yori JL, Seachrist DD, Johnson E, Lozada KL, Abdul-Karim FW, Chodosh LA, Schiemann WP, Keri RA. Kruppel-like factor 4 inhibits tumorigenic progression and metastasis in a mouse model of breast cancer. Neoplasia. 13:601–610. [PubMed: 21750654]
35. Gabizon A, Goren D, Horowitz AT, Tzemach D, Lossos A, Siegal T. Long-circulating liposomes for drug delivery in cancer therapy: a review of biodistribution studies in tumor-bearing animals. Adv Drug Deliv Rev. 1997; 24:337–344.
36. Rose PG. Pegylated liposomal doxorubicin: optimizing the dosing schedule in ovarian cancer. Oncologist. 2005; 10:205–214. [PubMed: 15793224]
37. Perou CM, Sorlie T, Eisen MB, van de Rijn M, Jeffrey SS, Rees CA, Pollack JR, Ross DT, Johnsen H, Akslen LA, Fluge O, Pergamenschikov A, Williams C, Zhu SX, Lonning PE, Borresen-Dale AL, Brown PO, Botstein D. Molecular portraits of human breast tumours. Nature. 2000; 406:747–752. [PubMed: 10963602]
38. Bertucci F, Finetti P, Birnbaum D. Basal breast cancer: a complex and deadly molecular subtype. Curr Mol Med. 2012; 12:96–110. [PubMed: 22082486]
39. Perreard L, Fan C, Quackenbush JF, Mullins M, Gauthier NP, Nelson E, Mone M, Hansen H, Buys SS, Rasmussen K, Orrico AR, Dreher D, Walters R, Parker J, Hu Z, He X, Palazzo JP, Olopade OI, Szabo A, Perou CM, Bernard PS. Classification and risk stratification of invasive breast carcinomas using a real-time quantitative RT-PCR assay. Breast Cancer Res. 2006; 8:R23. [PubMed: 16626501]
40. Bertucci F, Finetti P, Cervera N, Charafe-Jauffret E, Buttarelli M, Jacquemier J, Chaffanet M, Maraninchi D, Viens P, Birnbaum D. How different are luminal A and basal breast cancers? Int J Cancer. 2009; 124:1338–1348. [PubMed: 19058218]
41. Friedl P, Gilmour D. Collective cell migration in morphogenesis, regeneration and cancer. Nat Rev Mol Cell Biol. 2009; 10:445–457. [PubMed: 19546857]
42. Bidard FC, Pierga JY, Vincent-Salomon A, Poupon MF. A “class action” against the microenvironment: do cancer cells cooperate in metastasis? Cancer Metastasis Rev. 2008; 27:5–10. [PubMed: 18066649]
43. Kirfel G, Rigort A, Borm B, Herzog V. Cell migration: mechanisms of rear detachment and the formation of migration tracks. Eur J Cell Biol. 2004; 83:717–724. [PubMed: 15679116]
44. Kievit FM, Stephen ZR, Veiseh O, Arami H, Wang T, Lai VP, Park JO, Ellenbogen RG, Disis ML, Zhang M. Targeting of primary breast cancers and metastases in a transgenic mouse model using rationally designed multifunctional SPIONs. ACS Nano. 2012; 6:2591–2601. [PubMed: 22324543]
45. Shapiro, EGaM. Particles in a Shear Flow Near a Solid Wall: Effect of Nonsphericity on Forces and Velocities. Int J Multiphase Flow. 1996

46. Decuzzi P, Lee S, Bhushan B, Ferrari M. A theoretical model for the margination of particles within blood vessels. Ann Biomed Eng. 2005; 33:179–190. [PubMed: 15771271]

47. Gavze E, Shapiro M. Motion of inertial spheroidal particles in a shear flow near a solid wall with special application to aerosol transport in microgravity. Journal of Fluid Mechanics. 1998; 371:59–79.

48. Lee SY, Ferrari M, Decuzzi P. Shaping nano-/micro-particles for enhanced vascular interaction in laminar flows. Nanotechnology. 2009; 20:495101, 11. [PubMed: 19904027]

49. Gentile F, Chiappini C, Fine D, Bhavane RC, Peluccio MS, Cheng MM, Liu X, Ferrari M, Decuzzi P. The effect of shape on the margination dynamics of non-neutrally buoyant particles in two-dimensional shear flows. J Biomech. 2008; 41:2312–2318. [PubMed: 18571181]

50. Decuzzi P, Ferrari M. The adhesive strength of non-spherical particles mediated by specific interactions. Biomaterials. 2006; 27:5307–5314. [PubMed: 16797691]

51. Brazel CS. Magnetothermally-responsive nanomaterials: combining magnetic nanostructures and thermally-sensitive polymers for triggered drug release. Pharm Res. 2009; 26:644–656. [PubMed: 19005741]

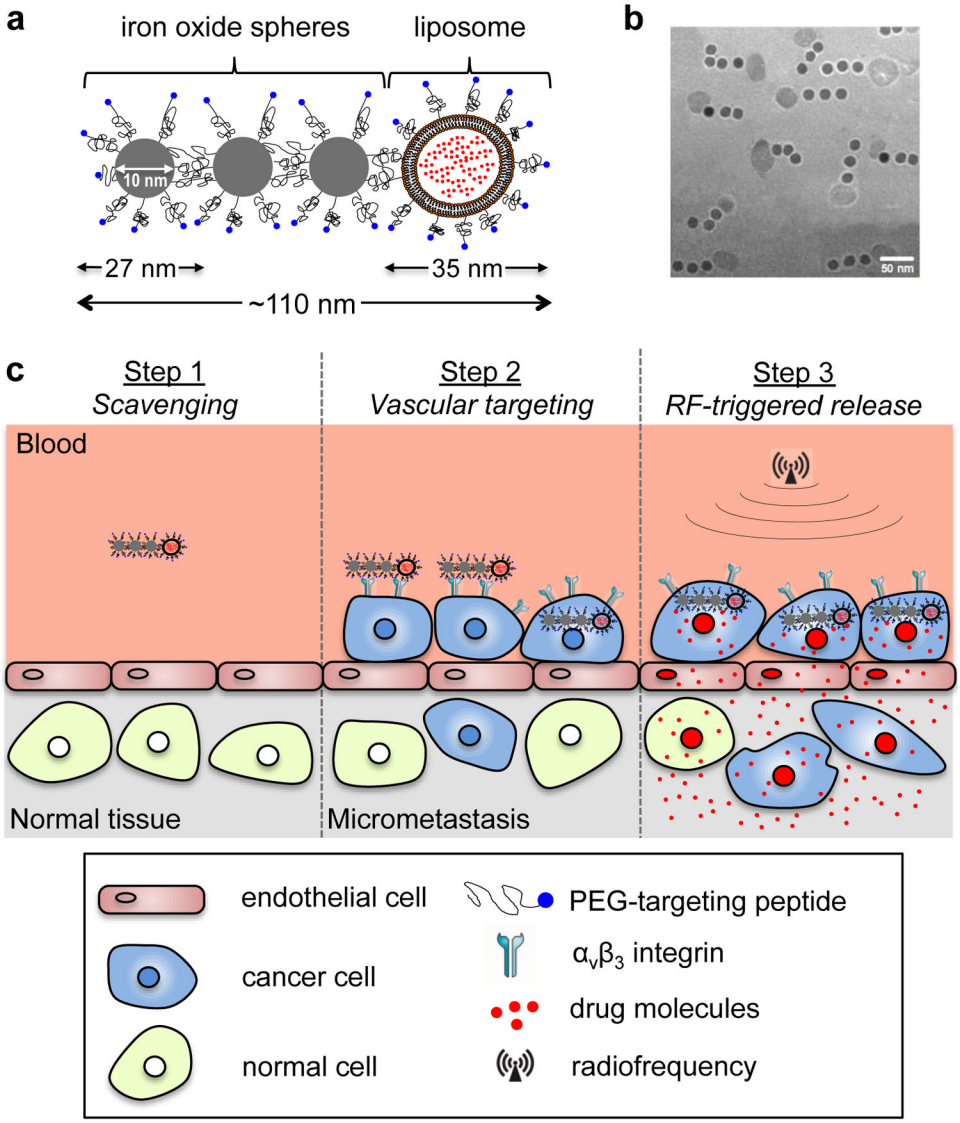

Fig. 1.

Illustration of the nChain particle and its therapeutic effect on micrometastasis. (a) Schematic of a linear nChain particle composed of three IO nanospheres and one drug-loaded liposome. (b) TEM image of nChain particles. (c) Illustration of the successful delivery of nanochain-based drug to metastasis via vascular targeting and RF-triggered drug release.

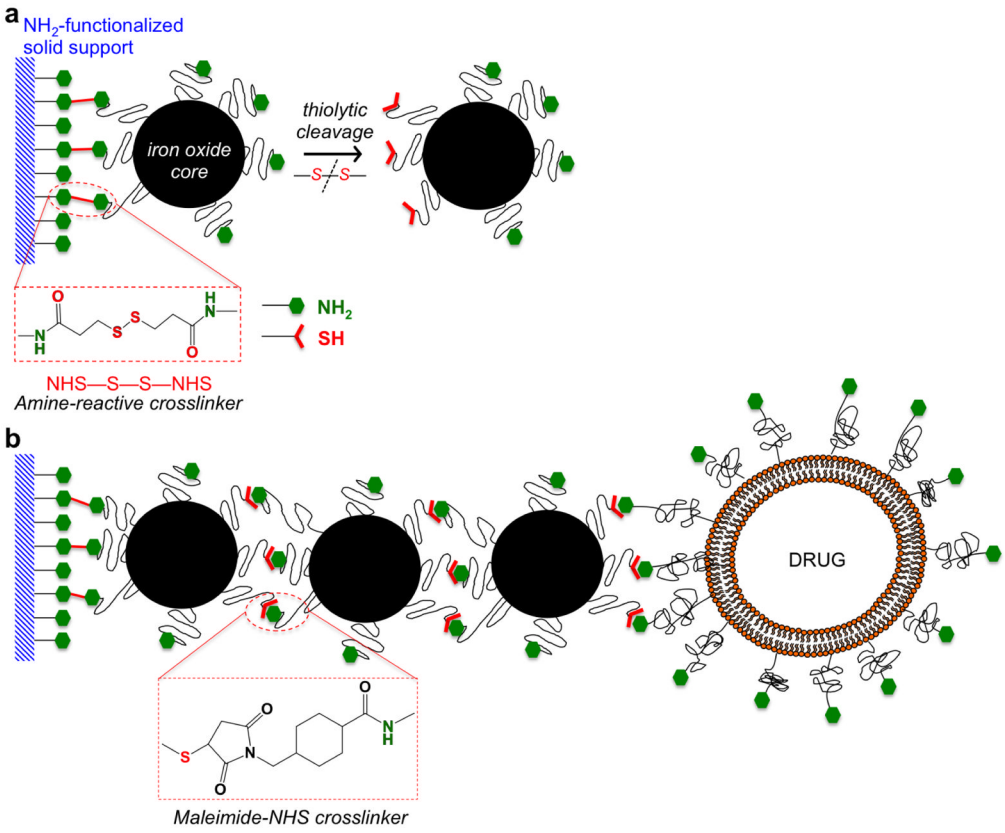

Fig. 2.

Reaction scheme of the controlled assembly of multicomponent nChain particles using solid-phase chemistry. (a) In the first step, chemical bifunctionality on the surface of parent IO nanospheres is topologically controlled resulting in nanospheres with two faces, one displaying only amines and the other only thiols. (b) In the second step, the two unique faces on the parent nanosphere serve as fittings to chemically assemble them into nanochains.

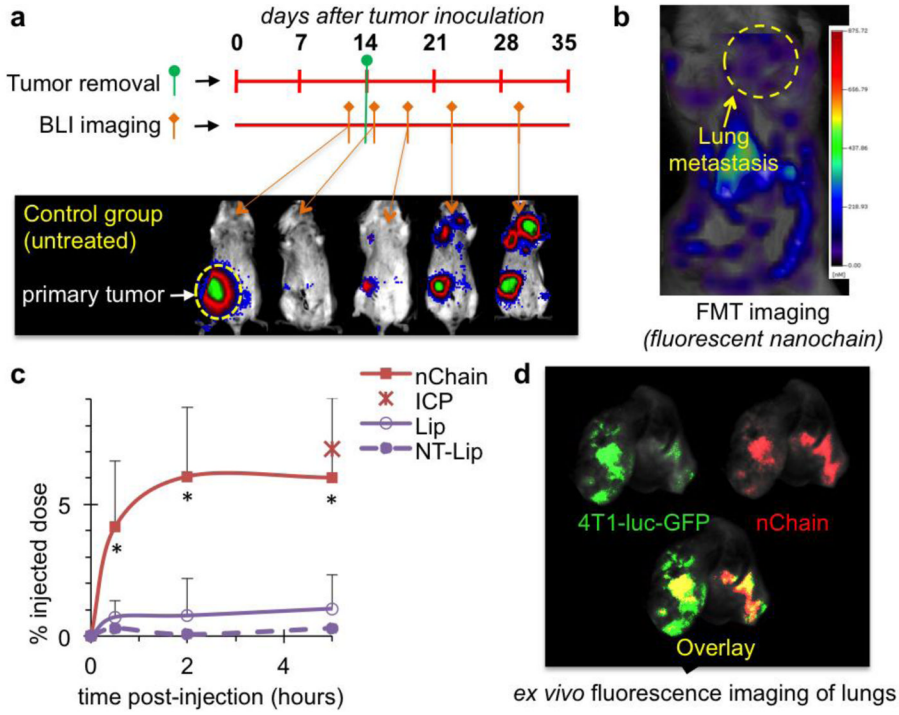

Fig. 3.

Evaluation of the ability of nChain particles to target metastasis in vivo. (a) The timeline of surgery and BLI imaging are shown with respect to implantation of 4T1 cancer cells into the mammary fat pad of female BALB/c mice. Representative BLI images of an untreated animal indicate the progression of metastatic disease. (b) Representative FMT images of the same mouse show the accumulation of nChain particles in lung metastasis at 2 h post-injection. The nChain particles were injected 11 days after surgical removal of primary tumor (25 days after tumor inoculation), which was the time point of early onset of lung metastasis. (c) Using an NIR fluorophore as a label, the time-course of nanoparticle accumulation in lung metastases was obtained by quantification of the fluorescence signal in the FMT images of mice injected with nChain, integrin-targeting liposome (Lip) and non-targeting liposome (NT-Lip) at a DOX dose of 0.5 mg/kg b.w. (n=4 mice in each group; * $P<0.02$ by Student's t-test). The lungs of the animals injected with nChain were excised and digested 5 h after administration and the iron concentration was measured using ICP-OES (data point indicated as ICP in the graph). Control animals were used to correct for background levels of endogenous iron. (d) Using a CRi Maestro fluorescence imaging system, ex vivo imaging of lungs 5 h after injection indicated the colocalization of nChain particles and 4T1 metastatic cells expressing GFP.

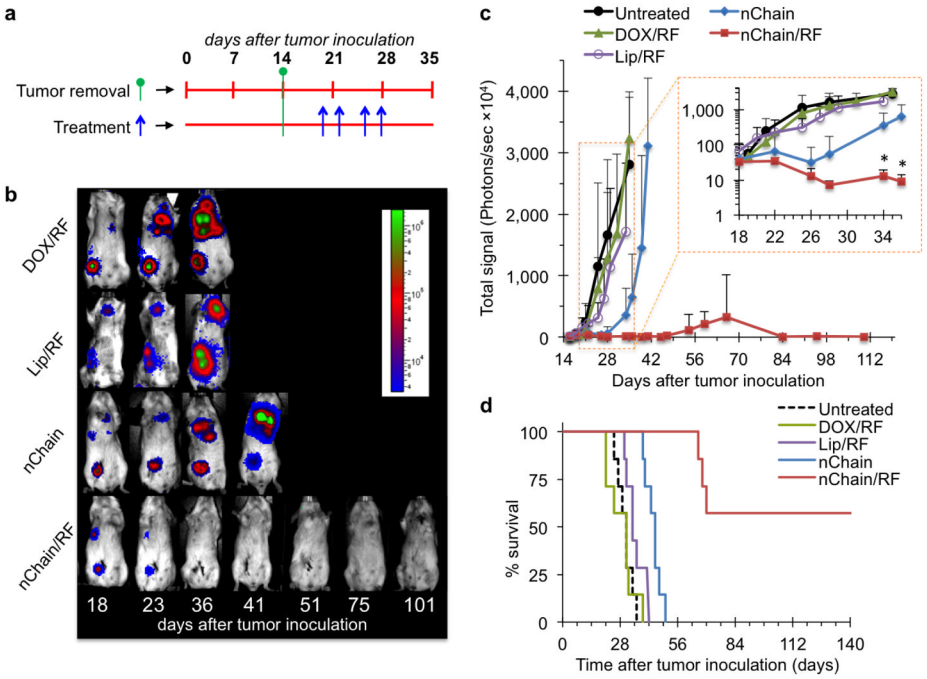

Fig. 4.

Treatment of breast cancer metastasis using the 4T1 mammary model in mice. (a) The timeline of surgery and schedule of treatments are shown with respect to tumor inoculation. (b) The response of cancer metastasis to treatment was monitored using longitudinal BLI imaging. Representative images are shown for animals treated with DOX/RF, Lip/RF, nChain and nChain/RF. In the case of treatments combined with the RF field, 45 min post-injection, animals were exposed for 60 min to an RF field (amplitude B=6.3 mT, frequency f=10 kHz) using a custom-made solenoid coil. All nanoparticle formulations were administered at 0.5 mg/kg DOX, while free DOX was injected at 5 mg/kg. (c) Quantification of the whole body BLI light emission is shown for the nChain/RF treatment and control treatments including nChain, DOX/RF and Lip/RF. The inset shows the same plot with the y-axis being in logarithmic scale (n=7 mice in each group; * $P<0.03$ by Student's t-test). (d) The survival time of the animals treated with nChain/RF, nChain, DOX/RF and Lip/RF is compared to that of the untreated group.

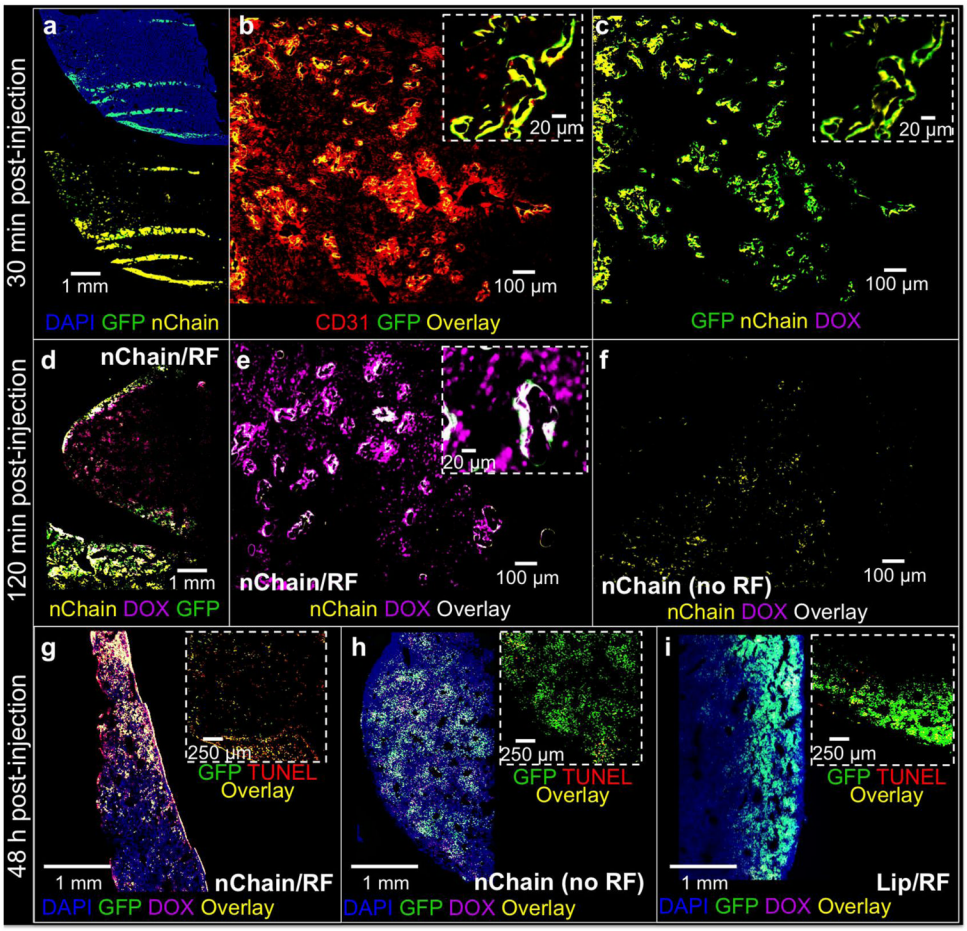

Fig. 5.

Histological evaluation of the anticancer effect of the nChain particle on micrometastasis in the liver. (a) Fluorescence imaging of an entire histological section of a lobe of liver 30 min after systemic administration of nChain at 0.5 mg DOX/kg b.w. Nuclei were stained with DAPI (5x magnification). Images of entire histological sections of the organ were obtained using the automated tiling function of the microscope. At 30 min post-injection, the location of metastatic cancer cells is shown with respect to the location of endothelial cells (b), nChain particles and DOX (c) in the same histological section (10x magnification; insets: 20x magnification). (d) At 120 min post-injection, fluorescence imaging of an entire histological section shows the widespread distribution of DOX molecules after a 60-min application of RF employed at 45 min post-injection (5x magnification). At 120 min post-injection, higher magnification imaging shows the distribution of DOX molecules with (e) or without RF (f) with respect to the location of cancer cells and nChain particles (10x magnification; inset: 20x magnification). At 48 h post-injection, fluorescence imaging of entire histological sections shows the distribution of DOX molecules with respect to cancer cells for the nChain/RF (g), nChain (h) and Lip/RF treatment (i). Insets show apoptotic cells in a small portion of the same images. Apoptotic cell nuclei were stained with TUNEL.

Table 1

Summary of different formulations and therapeutic protocols and their abbreviations

Abbreviation	Formulation	Therapeutic protocol
nChain	$\alpha_v\beta_3$ integrin-targeting nChain nanochains	no radiofrequency (RF) application
nChain/RF	$\alpha_v\beta_3$ integrin-targeting nChain nanochains	45 min after injection of the formulation, the RF field was applied for 60 min
NT-nChain	non-targeted nanochains	no RF application
Lip	$\alpha_v\beta_3$ integrin-targeting 35-nm liposome	no RF application
Lip/RF	$\alpha_v\beta_3$ integrin-targeting 35-nm liposome	45 min after injection of the formulation, the RF field was applied for 60 min
NT-Lip	non-targeted 35-nm liposome	no RF application
DOX/RF	free doxorubicin	45 min after injection of the formulation, the RF field was applied for 60 min